Study on the Biochar Yield and Heat Required during Pyrolysis of Two-Phase Olive Mill Waste

Joan J. Manyà[*]*, Sergio Laguarta, Miguel A. Ortigosa*

Thermo-chemical Processes Group (GPT), Aragón Institute of Engineering Research (I3A), University of Zaragoza, Technological College of Huesca, crta. Cuarte s/n, E-22071, Huesca, Spain

KEYWORDS

Pyrolysis; Two-Phase Olive Mill Waste; Heat Demand; Kinetics; Secondary Charcoal.

ABSTRACT

The present study analyzes the effect of several operating factors (initial sample mass, heating rate, conditions of the crucible, and inorganic matter content) on the pyrolysis of two-phase olive mill waste. Simultaneous TGA-DSC measurements were performed according to a one-half fractional factorial design to obtain statistically significant conclusions. The results from this screening design pointed out that the behavior of the TPOMW pyrolysis process is statistically affected, to a greater or lesser extent, by the four factors analyzed. The factors related to the promotion of secondary charring reactions (the initial sample mass and the conditions of the crucible) had the main influence on both the apparent heat and charcoal yield. The enhancement of the charring reactions implies a dramatic decrease of the apparent heat of pyrolysis: from highly endothermic (2559 ± 100 kJ kg^{-1}) to slightly exothermic (–44.2 ± 49 kJ kg^{-1}). On the other hand, a new approach is proposed to modeling the apparent kinetics of TPOMW pyrolysis (both primary decomposition and secondary charcoal production). The performance of this approach is good enough to provide satisfactory estimations of a large number of unknown kinetic parameters in very short computational times.

1. Introduction

After years of several technology efforts aimed at saving water during the olive oil extraction phase, an alternative centrifugation system was developed which greatly reduced olive mill wastes. This system is known as "two-phase", because it produces two fractions: sludge (two-phase olive mill waste or "alperujo") and olive oil.[1, 2] Two-phase olive mill waste (TPOMW) is an acidic and wet solid waste, the disposal of which is a considerable problem for olive oil processors. TPOMW is sometimes used as a soil amendment after a compositing process.[3, 4] As an alternative pathway for managing this waste, TPOMW can be pyrolyzed for biochar purposes.

Biochar is a carbon-rich substance, which can be produced by slow pyrolysis at relatively low temperatures (< 700 °C). The definition adopted by the International Biochar Initiative (IBI) furthermore specifies the need for purposeful application of this material to soil for both agricultural and environmental gains.[5] Primary pyrolysis involves a cracking process to convert the biomass into charcoal (biochar), permanent gas species (e.g.; CO_2, CO, and light hydrocarbons), and condensable vapors at room conditions (water and organic compounds). Among other operational factors, heating rate plays an important role in the process. It is usually assumed that the charcoal yield is expected to increase as the heating rate becomes lower. For this reason, slow pyrolysis processes, in which the biomass feedstock is heated at a rate usually ranged from 5 to 30 K min^{-1}, are commonly used for producing charcoal.[6, 7]

As noted in numerous early studies,[8-11] several factors, in addition to heating rate, can affect charcoal yield; among these are peak temperature, vapor residence time, and inorganic matter content. Peak temperature is defined as the highest temperature reached during the pyrolysis process.[6] As a general rule, charcoal yield decreases as peak temperature increases. Regarding

the vapor residence time, an increase of which seems to enhance secondary charcoal production, because of the repolymerization of the primary organic vapors onto the solid carbonaceous matrix.[6, 9] This effect is sometimes confounded with the intrinsic effect of pressure when pyrolysis tests are conducted under different pressures at a constant inert gas flow rate.[12] Referring to the inorganic matter content, special attention was focused on discussing its influence on pyrolysis product distribution. During biomass pyrolysis, inorganic matter, especially alkali and alkali earth metals (AAEM), can catalyze both biomass decomposition and char forming reactions.[13] In light with this, several studies reported lower charcoal yields when the biomass feedstock was leached with water as a measure to partially remove inorganic matter.[14-18]

Detailed knowledge of kinetics and heat requirement for biomass pyrolysis is needed in order to design and scale-up reliable pyrolysis reactors. Most of the current kinetic studies on pyrolysis of biomass are based on experiments involving thermogravimetric measurements. Nevertheless, the current models are unable to establish a generically mechanism for the pyrolysis process of biomass.[19] This fact is due to the effect on experimental results of the intrinsic properties of the biomass feedstock (i.e., lignin content), the operating conditions (i.e., sample size and heating rate), and the mathematical treatment used to evaluate the data.[20, 21]

Regarding the heat involved during biomass pyrolysis, a wide range of measured values have been reported in literature varying from endothermic to exothermic.[6, 22-24] This variability in results is attributed to the effects of both the operating conditions (during calorimetric experiments) and biomass composition. As mentioned above, the composition of a given biomass feedstock strongly affects the behavior of the pyrolysis process. Thus, differences in hemicellulose, cellulose, lignin, extractives, and inorganic matter contents result in variations of

heat required or released during the progress of thermal decomposition. In this sense, Haykiri-Acma and coworkers[25] analyzed the thermal behavior of chemically isolated hollocelulose (hemicellulose + cellulose) and lignin from hazelnut shells. They observed that both lignin and hollocellulose produced heat during pyrolysis. This finding suggests that some kind of competition exists between exothermic char formation and endothermic volatile formation pathways. Inorganic matter can play a crucial role in shifting the balance in favor of heat release, due to its catalytic effect which simultaneously reduces the energy requirements for the volatilization of polymers and promotes the exothermic secondary char formation.[26, 27] In addition to the nature of the biomass feedstock, the experimental conditions under which DSC (differential scanning calorimetry) measurements are conducted also influence heat results. More in detail, the initial sample mass and the conditions of the crucible (with or without a lid) are strongly related to vapor-solid secondary interactions and, consequently, to both charcoal yield and measured heat. In line with this, Gómez and coworkers[23] observed high alterations in the heat demand (from endothermicity to exothermicity) when they varied the initial sample mass (in the range 2–10 mg) and/or replaced the crucible without lid by a covered one.

The goal of the present study is to analyze the effect of several factors on both charcoal yield and measured heat during pyrolysis of TPOMW. These factors are: initial sample mass, heating rate, conditions of the crucible (covered or uncovered), and inorganic matter content. For this purpose, a fractional factorial design of experiments approach was performed in order to establish statistically significant conclusions. Experimental runs were conducted in a simultaneous TG-DSC apparatus under atmospheric pressure. As an additional contribution of the present study, kinetic parameters of both primary pyrolysis and secondary char formation were estimated.

2. Experimental section

2.1. Materials. The TPOMW samples were collected from an extra-virgin olive oil factory located in the Spanish region of Aragón. In that factory, two-phase olive mill wastes were sun-dried in the field for several months (final moisture content: 10–15%). The as-received samples were broken in a jaw crusher and sieved to obtain a particle size in the range of 0.25–2.5 cm. To partially remove AAEM species from the raw biomass samples, a water leaching procedure was carried out. Approximately 5 g of sample was immersed in 1 L of ultrapure water (resistivity > 18.2 MΩ cm^{-1}) at room temperature and stirred for 24 h.[28] Table 1 reports the proximate and ultimate analyses of both raw and washed samples. Regarding the inorganic matter composition, a Thermo Electron ARL ADVANTXP+ XRF spectrometer was used to determine the ash composition, based on the weight fractions of the equivalent oxides[29], according to the ASTM standard D4326-04. Results from the X-ray fluorescence (XRF) analyses, which are shown in Table 1, are consistent with earlier measurements for biomass materials reported in the literature[28, 30]. This fact suggests that water leaching was useful to almost completely remove some species (K and Cl) and partially remove other ones (i.e., Ca and Mg).

2.2. Simultaneous TG-DSC apparatus. Pyrolysis runs were performed using a STA 449 F3 Jupiter (Netzsch, Germany), which comprises a robust and accurate system for both TGA and DSC measurements (resolution of 0.1 μg and 1.0 μW, respectively). A platinum-rhodium crucible (with or without lid), which can contain up to 45 mg of sample, was used for all experiments. The inert atmosphere was maintained using nitrogen at a flow rate of 50 mL (NTP) min^{-1} under an absolute pressure of 125 kPa. Both DSC and TGA curves were obtained by heating samples from room temperature to 600 °C following a linear program. Temperature was kept constant at 110 ºC for 30 min to ensure the complete drying. Final temperature was also

kept constant during 60 min to achieve a stable final mass. All TGA and DSC results reported in this study were corrected by the baseline obtained from runs performed with empty crucibles under the same operating conditions (blank runs).

2.3. Design of experiments. To statistically analyze the effects of the selected factors, a twice replicated two-level fractional factorial design was established.[31] This kind of design is very useful to identify the factors with large effects in relatively few experiments. More in detail, the adopted design of experiments was a one-half fraction of the full factorial design with a resolution of IV. Thus, no main effect can be aliased with any other main effect or with any two-factor interaction, but some two-factor interactions can be aliased with each other.[31] The levels of studied factors, which are summarized in Table 2, were the following: initial sample mass (10 and 40 mg), linear heating rate (5 and 25 K min^{-1}), conditions of the crucible used (uncovered or covered), and type of sample (untreated or washed). By following this approach, the total number of TGA-DSC runs was 16 (2 replicates × 0.5 × 2^4). To create the randomized design of experiments and perform the appropriate statistical analyses, the RcmdrPlugin.DoE package[32] within R environment (version 3.0.0) was used. Table 2 displays the created design.

3. Results and discussion

3.1. Data processing. The main experimental results are summarized in Table 3, which reports the measured values of the charcoal yield (y_{char}), maximum-rate temperature (T_{max}), and apparent heat (Q_{exp}). The charcoal yield is defined as the ratio between m_{char} (mass of produced charcoal after 60 min at 600 ºC) and m_{bio} (dry mass of feedstock after 30 min at 110 ºC). T_{max} corresponds to the temperature at which the maximum rate of weight loss was reached (the overall maximum of the sign-changed derivative mass-loss curve) and is closely related to the devolatilization

reactivity of the solid material.[12] Regarding the apparent heat involved in the pyrolysis process (Q_{exp}), the values shown in Table 3 were calculated by integrating the DSC curve and thus are the sum of three components: the energy necessary to heat the sample, the latent heat of vaporization of the condensable fraction (bio-oil) and the heat involved in reactions. Interactions among these terms become inevitable and it seems very complicated to separate them apart. For this reason, and in agreement with a previous study of He and coworkers[33], the integrated value of the DSC curve can be considered as an approximation of the caloric requirement of the pyrolysis process. Many previous studies (see, for instance the works of Gómez et al.[23] and Van de Velden et al.[34]) have tried to systematically estimate the energy necessary to heat the sample without considering the thermal effects of the pyrolysis reaction. This step involves the use of specific heat values, for both biomass and char, based on multiple hypotheses. More recently, Yang and coworkers[35] have proposed a method to estimate the heat required for biomass pyrolysis as the enthalpy difference between the products at the peak temperature and the biomass at 298.15 K. This method, however, requires knowledge of bio-oil yield, which cannot be measured in a simultaneous TG-DSC apparatus.

An example of both TGA and DSC curves is illustrated in Figure 1. For each experimental run conducted, normalized TGA curve ($m_{norm} = m_t/m_{bio}$) was differentiated to obtain the corresponding DTG curve and T_{max} value (see Figure 2 for an example). With regard to the DSC signal, the "Peak Analyzer" tool implemented in OriginPro 8.5 (OriginLab, MA) was used to identify peaks, define the shape of the baseline and then integrate the heat flow signal as the sum of the areas of all identified peaks. The value of the computed integral divided by the initial dry mass (m_{bio}) corresponds to the Q_{exp} value in kJ kg^{-1}. Figure 3 shows two examples of DSC signal

integration, one with a single endothermic peak and one involving several endothermic and exothermic peaks.

3.2. Statistical analysis. Results displayed in Table 3 were statistically analyzed to determine the effects of the factors described above. The computed apparent heat (Q_{exp}) values show a great variability depending on the applied treatment. The highest values (highly endothermic, 2559 ± 100 kJ kg^{-1}) were obtained when all the factors were maintained at their low levels (low sample mass, low heating rate, uncovered crucible, and raw biomass). It should be noted that this high value corresponds to an apparent heat of pyrolysis, because also includes the energy required to heat the sample and vaporize the volatile matter. For this reason, a direct comparison between the data reported here and literature values is complex. In this sense, Van de Velden and coworkers[34] estimated that the heat of pyrolysis, deduced from DSC measurements, for several biomass feedstocks (among which TPOMW was not included) ranged from 207 to 434 kJ kg^{-1}. However, in the above-mentioned study of Yang and coworkers[35], a value of 1300–1600 kJ kg^{-1} was estimated for the heat of pyrolysis of five different biomass samples (cedar, pine, willow, bamboo, and sasa bamboo).

Table 4 reports the regression coefficients and the ANOVA table for the apparent heat. All of the factors considered in the present study have significant effects on the value of Q_{exp}. An increase of sample mass (factor A) leads to a significant decrease in apparent heat. This finding suggests that when an initial sample mass of around 40 mg was used, exothermic char formation was promoted due to an increase of resistance to volatile diffusion. The Q_{exp} values also decreased when the linear heating rate (factor B) changed from 5 to 25 K min^{-1}. This effect on heat demand, quantitatively much smaller than those observed for factor A, could be explained in part by heat transfer limitations. In this sense, as heating rate increases the temperature gradient

across the solid particles can also increases, causing a displacement of the maximum decomposition rate towards higher temperatures.[36, 37] Regarding the factor C (crucible with or without a lid), its effect on decreasing the apparent heat is the largest, as shown in Table 4. As reported in previous studies[22, 23], enhancing the contact time between the volatiles and the primary char can promote secondary char formation, which is strongly exothermic. The last factor analyzed (factor D related to the role of the water-soluble inorganic fraction) has the smallest effect on reducing the apparent heat. In a similar way as previously mentioned for the heating rate, the partial removal of AAEM can reduce the rate of the devolatilization process and displace the peak rate towards higher temperatures. Table 4 also reports the regression coefficients for the two-way interactions terms. The alias structure of the applied design shows that the aliases among 2-factor interactions are the following: AB + CD; AC + BD; and AD `+ BC. In this context, the interpretation of statistical results for 2-factor interactions becomes difficult. However, some qualitative considerations can be drawn by observing the interaction plots. As seen in Figure 4a, the interaction between factors B and D seems to be significant and should be quantitatively evaluated in further designs of experiments (full-factorial and/or central composite designs).

Concerning the charcoal yield, Table 5 shows the results of statistical analysis. It should be noted that only the main effects of two of the four factors (factor A and C) are statistically significant at a confidence level of 95%. Both increasing the initial mass of TPOMW sample and covering the crucible result to a significant increase of charcoal yield. This finding is consistent with literature data (see, for instance, the published studies of Gómez et al.[23], and Rath et al.[22]) and can be explained by the enhancement of secondary reactions between the primary volatiles and the solid residue. Assuming this fact as true, it seems reasonable to suggest that high

charcoal yields might be associated to low values of apparent heat. Nevertheless, the result of Pearson's correlation test reveals that there is no significant linear correlation between Q_{exp} and y_{char} variables (null hypothesis of absence of correlation cannot be rejected at a significance level of 0.05). This fact, in addition to the relatively low value of the adjusted coefficient of determination (R^2_{adj} = 0.6320), could indicate that some curvature can exist in the response function.[31] Concerning the two-factor interaction terms, it should be noted that the effect of the AC (+BD) interaction term is the largest. As observed for the Q_{exp} response, the interaction plot between factors B and D given in Figure 4b suggests that this interaction term might be the main contributor to the overall two-factor interaction effect.

With regard to the maximum-rate temperature (T_{max}), the results of the statistical analysis, which are given in Table 6, suggest that this response variable is mainly affected by both the heating rate and the conditions of the crucible used. The effect of factor B, which results in a significant increase of the maximum-rate temperature, confirms the above-mentioned assumption that increasing heating rate causes a displacement of the highest decomposition rate towards higher temperatures. Special attention should be focused on the factor C, the effect of which is quantitatively similar to those of factor B. This observed behavior might indicate that char formation plays an important role in the relatively low temperature region. In other words, an exothermic behavior prevails at the initial stage of the process. However, and as can be seen in Table 6, an increase of the initial mass has no significant influence on the maximum-rate temperature. This fact could suggest that the thermal effect of the enhancement of secondary charring reactions depends on the approach adopted to promote the residence time of the primary vapors. In the case of factor D, a significant effect on T_{max} is reported in Table 6. As mentioned before, an increase of the maximum-rate temperature can be expected when the AAEM is

partially removed. Nevertheless, the displacement of the peak rate is much lower than those estimated by factors B and C. Finally, Table 6 also reveals that the 2-factor interaction effect can be mainly attributed to the AD (+BC) interaction term. In this case, the shape of the corresponding interaction plots did not provide any qualitative information.

As a summary of this section, it should be highlighted that the behavior of the TPOMW pyrolysis process is statistically affected, to a greater or lesser extent, by the four factors analyzed. The factors A and C, which are related to the promotion of secondary charring reactions, have the main influence on both the apparent heat and charcoal yield. However, the other analyzed factors (B and D) cannot be excluded in further experimental designs, because the effect of the 2-way interaction terms between any two factors (including the factors B and D) could be statistically significant.

3.3. Kinetic parameters. The TGA experimental data were processed to estimate the kinetic parameters of the primary pyrolysis on the basis of a single reaction-order model.[36, 38] In this model, the reaction rate is proportional to the fraction of unreacted material raised to a specific exponent, which is known as the reaction order (n):[12]

$$\frac{d\alpha}{dT} = k(T)(1-\alpha)^n \tag{1}$$

where α is the conversion fraction of a solid sample:

$$\alpha = \frac{m_{bio} - m_t}{m_{bio} - m_{char}} \tag{2}$$

The reaction rate constant can be obtained assuming the Arrhenius equation:

$$k(T) = A\exp\left(\frac{-E}{RT}\right) \tag{3}$$

with A and E being the pre-exponential factor and the activation energy, respectively.

In addition to this, an approach based on the assumption that the overall decomposition of a biomass feedstock can be described by means of several independent parallel reactions is widely adopted by the research community.[6, 10, 39-42] By using this approach, the pyrolysis rate can be expressed as follows:

$$\frac{d\alpha}{dt} = \beta\frac{d\alpha}{dT} = \sum_{i=1}^{3} c_i A_i \exp\left(\frac{-E_i}{RT}\right)(1-\alpha_i)^{n_i} \tag{4}$$

where c_i represents the contribution of the ith partial reaction to the overall weight loss, whereas β corresponds to the linear heating rate. In the present study, it was assumed that the number of independent parallel reactions was 3. Thus, the overall weight loss of the samples can be calculated as the sum of the volatiles released from three pseudo-components:[43] hemicellulose (first pseudo-component), the major fraction of cellulose (second pseudo-component) and, as a third pseudo-component, the sum of lignin, the remaining fraction of cellulose, and other organic components (fats and other extractives).

The above-described model was implemented in MATLAB R2011b (Mathworks, MA) as a nonlinear grey-box model object ("idnlgrey" function). The state-space model structure involved 1 input variable (temperature), 3 state variables (the normalized mass loss for each pseudo-component, x_i), 1 output variable (the calculated normalized mass, m_{calc}), and 12 unknown parameters (c_i, A_i, E_i, and n_i), the values of which were estimated via a trust-region reflective

algorithm (the "lsqnonlin" MATLAB's function, which solves nonlinear least-squares curve fitting problems).[44] It is well known that there may exist multiple solutions to the nonlinear least-squares (NLS) minimization problem. [45] In other words, depending on the starting values adopted for the kinetic parameters, the iterative method can identify different local solutions.

In the present work, the initial values of the model parameters were estimated using a new approach, which is based on the peak deconvolution of the time derivative mass-loss curve (DTG curve) and on the sequential methodology proposed by Huang and coworkers.[20] As a first step of the used approach, the normalized –DTG curve was deconvoluted into three bi-Gaussian distributions (one for each pseudo-component) using the *Peak Analyzer* tool within OriginPro v. 8.5 (OriginLab Corporation, MA). In the second step, the reaction order corresponding to the primary pyrolysis for each pseudo-component was estimated by means of the regression equation deduced by Huang and coworkers:[20]

$$n_i = 0.1368 \exp[5.3635(1-\alpha_i)_{\max}] \tag{5}$$

where $(1-\alpha_i)_{max}$ is the "unreacted" area fraction of the *i*th peak at the maximum reaction rate and is deduced from the corresponding bi-Gaussian peak. Once the reaction order was estimated, the starting values of A_i and E_i were calculated using equations 6 and 7, which are based on the Kissinger's assumption, that is, the maximum reaction rate occurs when the first derivative of equation 1 is zero.[20]

$$E_i = n_i^{n_i/(n_i-1)} R T_{\max_i}^2 \left(\frac{d\alpha_i}{dT}\right)_{\max} \tag{6}$$

$$A_i = n_i^{\,n_i/(n_i-1)}\beta\left(\frac{d\alpha_i}{dT}\right)_{\max}\exp\left[n_i^{\,n_i/(n_i-1)}T_{\max_i}\left(\frac{d\alpha_i}{dT}\right)_{\max}\right] \quad (7)$$

Regarding the c_i parameters, their starting values were taken as the area fraction of the *i*th peak. Only experiments performed at a heating rate of 5 K min^{-1} were considered to avoid possible systematic errors due to heat transfer limitations.

In addition to the kinetic expressions for the primary pyrolysis, an additional reaction was considered to describe the secondary charcoal formation. Thus, the normalized sample mass can be estimated as follows:

$$\frac{dm_{calc}}{dt} = -\sum_{i=1}^{3} c_i A_i \exp\left(\frac{-E_i}{RT}\right)(1-\alpha_i)^{n_i} + A_{\text{sec}}\exp\left(\frac{-E_{\text{sec}}}{RT}\right)\left(\gamma\sum_{i=1}^{3}x_i\right)^{n_{\text{sec}}} \quad (8)$$

where A_{sec}, E_{sec}, and n_{sec} correspond to the kinetic parameters for the secondary solid-vapor interactions; whereas γ is the overall fraction of volatiles ($x_1 + x_2 + x_3$) that can be converted to charcoal via repolymerization. Due to the absence of similar data in the literature, in which the most available studies focused on secondary interactions only analyzed the cracking to gas species,[19] the starting values of A_{sec}, E_{sec}, n_{sec}, and γ were chosen to be 1.

Table 7 reports the estimated kinetic parameters (both starting and optimized values) from four experimental runs (#1, #4, #11, and #16). The kinetic model given by equation 4 was applied for run #1, whereas the model in equation 8 was assumed for the rest of runs, in which the applied treatment would be able to promote the formation of secondary charcoal. The values of the estimated activation energies for the three pseudo-components are within the wide range reported in the literature (see, for instance, the reviews of Di Blasi[19] and White et al.[36]) and relatively

close to those reported in a previous study using the same TPOMW samples.[12] In that study, which was performed using a CAHN TG-151 thermobalance at a linear heating rate of 5 K min^{-1}, the reported values for E_1, E_2, and E_3 were 109.5 ± 2.5, 167.4 ± 14.6, and 33.1 ± 0.2; respectively. The differences in the estimated activation energy values might be due to differences in the experimental conditions (i.e., initial sample mass and position of thermocouple), the mathematical treatment of the data, and the compensation effect among kinetic parameters (which is difficult to avoid in practice).

Regarding the reliability of the kinetic approach, it should be highlighted that the statistical significance of the estimated parameters could not be evaluated, due to possible singularities of the covariance matrix. Consequently, confidence intervals for the model parameters were not computed (applying bootstrap procedures can be a way to estimate the precision of the parameters, but it's a very time-consuming technique). In other words, the set of model parameters estimated here for each experiment is not necessarily the only one that can fit the data. However, in spite of this statistical uncertainty, the kinetic approach adopted in the present study seems to be a convenient way to estimate the kinetics of both primary and secondary pyrolysis processes in terms of charcoal yield. To support this claim, Table 7 reports very high values of adjusted R^2 (0.9902–0.9940) and very small values of FPE (Akaike's final prediction error). Figure 5 displays two examples of the quality of the fit provided by equation 4 for run #1, and by equation 8 for run #4.

At this point, it would be interesting to determine if a robust relationship between the secondary charcoal formation and the apparent heat released can be established. The challenge is particularly difficult due to the complexity of the pyrolysis process and the possible presence of noise factors and/or noise factor interactions. Nevertheless, some interesting observations can be

made from Figure 6, which simultaneously shows the rate of secondary charcoal production (calculated using equation 8) and the specific heat flow signal for experimental runs #11 and #16. As can be seen in Figure 6, it seems reasonable to assume that the kinetic approach used in the present study is able to obtain an estimate of the secondary charcoal production consistent with the experimentally observed exothermic behavior. However, further studies are required to critically evaluate the performance of the proposed approach.

4. Conclusions

The main conclusions and suggestions to be drawn from this study can be summarized as follows:

The results from the design of experiments provide statistically supportable evidence regarding the effects of the four selected operating parameters on the TPOMW pyrolysis behavior. As expected, an increase of the initial sample mass and/or the use of a covered crucible are measures which lead to the promotion of charcoal formation. This enhancement of the charring reactions implies a dramatic decrease of the apparent heat of pyrolysis, which is also affected by the heating rate and the greater or lesser presence of AAEM species. Further studies are needed to clarify the effects of the 2-way interaction terms.

The proposed approach to modeling the apparent kinetics of TPOMW pyrolysis (both primary decomposition and secondary charcoal production) is able to provide satisfactory estimations of a large number of unknown parameters in very short computational times. Nevertheless, further efforts are required to assess the statistical significance of the estimated parameters (by implementing bootstrap or other resampling procedures).

Establishing a quantitative relationship between the secondary charcoal production and the heat involved in the process should be a priority objective for the research community. The findings reported here indicate that the evolution of the heat involved during pyrolysis can be partially related to the formation of secondary charcoal. However, additional research tasks are required to build a predictive model to estimate both charcoal yield and heat involved as a function of the operating conditions. Among these tasks, the formulation of accurate regression models from the data collected through the more advanced designs of experiments (full factorial and/or central composite designs) could be a useful and powerful tool for achieving this goal.

Author information

*E-mail: joanjoma@unizar.es

Acknowledgements

J.J.M. gratefully acknowledges the financial support from Spain's State Secretariat for Research (Project ENE2011-22657).

Nomenclature

A: Pre-exponential factor of the Arrhenius equation (s^{-1}).

c: Contribution of a given pseudo-component to the overall weight loss (mass fraction).

E: Activation energy (J mol^{-1}).

m_{bio}: Dry mass of TPOMW sample after 30 min at 110 ºC (mg).

m_{calc}: Normalized sample mass estimated by the kinetic model (–).

m_{char}: Mass of produced charcoal after 60 min at the given peak temperature (mg).

m_{norm}: Experimental normalized sample mass (–).

m_t: Experimental sample mass as a function of time (mg).

n: Reaction order.

Q_{exp}: Apparent heat involved in the pyrolysis process (kJ kg^{-1}).

T_{max}: Temperature at which the maximum rate of weight loss is reached (°C).

x: Normalized mass of volatiles released (–).

y_{char}: Charcoal yield (mass fraction).

Greek symbols

α: Conversion of the overall devolatilisation process.

β: Linear heating rate (K min^{-1}).

γ: Overall mass fraction of volatiles that can be converted to charcoal via repolymerization.

Subscripts

i: ith pseudo-component.

sec: Secondary charring reaction.

Acronyms

AAEM: Alkali and Alkali Earth Metals.

DSC: Differential Scanning Calorimetry.

DTG: Differential Thermogravimetric Analysis.

FPE: Akaike's Final Prediction Error.

NLS: Nonlinear Least Squares.

TGA: Thermogravimetric Analysis.

TPOMW: Two-Phase Oil Mill Waste.

XRF: X-ray fluorescence.

References

(1) Roig, A.; Cayuela, M. L.; Sánchez-Monedero, M. A. *Waste Manage.* **2006**, *26*, 960–969.

(2) Cayuela, M. L.; Millner, P. D.; Meyer, S. L. F.; Roig, A. *Sci. Total Environ.* **2008**, *399*, 11–18.

(3) Alburquerque, J. A.; Gonzalvez, J.; Garcia, D.; Cegarra, J. *Process Biochemistry* **2006**, *41*, 127–132.

(4) Ruggieri, L.; Cadena, E.; Martinez-Blanco, J.; Gasol, C. M.; Rieradevall, J.; Gabarrell, X.; Gea, T.; Sort, X.; Sanchez, A. J. *Clean. Prod.* **2009**, *17*, 830–838.

(5) Lehmann, J.; Joseph, S. Biochar for Environmental Management: An Introduction. In *Biochar for Environmental Management: Science and Technology*; Lehmann, J., Joseph, S., Eds.; Earthscan: London, 2009; Vol. 1, pp 1–10.

(6) Antal, M. J.; Gronli, M. *Ind. Eng. Chem. Res.* **2003**, *42*, 1619–1640.

(7) Zhang, L.; Chunbao, X.; Champagne, P. *Energy Conv. Manage.* **2010**, *51*, 969–982.

(8) Di Blasi, C.; Signorelli, G.; Di Russo, C.; Rea, G. *Ind. Eng. Chem. Res.* **1999**, *38*, 2216–2224.

(9) Antal, M. J.; Croiset, E.; Dai, X.; DeAlmeida, C.; Mok, W. S.; Niclas, N.; Richard, J. R.; Al Majthoub, M. *Energy Fuels* **1996**, *10*, 652–658.

(10) Manyà, J. J.; Ruiz, J.; Arauzo, J. *Ind. Eng. Chem. Res.* **2007**, *46*, 9061–9070.

(11) Demirbas, A. *J. Anal. Appl. Pyrolysis* **2004**, *72*, 243–248.

(12) Manyà, J. J.; Roca, F. X.; Perales, J. F. *J. Anal. Appl. Pyrolysis* **2012**, in press; DOI 10.1016/j.jaap.2012.10.006.

(13) Yaman, S. *Energy Conv. Manage*. **2004**, *45*, 651–671.

(14) Teng, H.; Wei, Y. C. *Ind. Eng. Chem. Res.* **1998**, *37*, 3806–3811.

(15) Jensen, P. A.; Frandsen, F. J.; Dam-Johansen, K.; Sander, B. *Energy Fuels* **2000**, *14*, 1280–1285.

(16) Manyà, J. J.; Velo, E.; Puigjaner, L. *Ind. Eng. Chem. Res.* **2003**, *42*, 434–441.

(17) Meszaros, E.; Jakab, E.; Varhegyi, G.; Szepesvary, P.; Marosvolgyi, B. *J Anal. Appl. Pyrolysis* **2004**, *72*, 317–328.

(18) Gomez, C. J.; Manyà, J. J.; Velo, E.; Puigjaner, L. *Ind. Eng. Chem. Res.* **2004**, *43*, 901–906.

(19) Di Blasi, C. *Progress Energy Comb. Sci.* **2008**, *34*, 47–90.

(20) Huang, Y. F.; Kuan, W. H.; Chiueh, P. T.; Lo, S. L. *Bioresour. Technol.* **2011**, *102*, 9241–9246.

(21) Burhenne, L.; Messmer, J.; Aicher, T.; Laborie, M. *J. Anal. Appl. Pyrolysis* **2013**, *101*, 177–184.

(22) Rath, J.; Wolfinger, M. G.; Steiner, G.; Krammer, G.; Barontini, F.; Cozzani, V. *Fuel* **2003**, *82*, 81–91.

(23) Gomez, C.; Velo, E.; Barontini, F.; Cozzani, V. *Ind. Eng. Chem. Res*. **2009**, *48*, 10222–10233.

(24) Bates, R. B.; Ghoniem, A. F. *Bioresour. Technol.* **2013**, *134*, 331–340.

(25) Haykiri-Acma, H.; Yaman, S.; Kucukbayrak, S. *Fuel Process Technol.* **2010**, *91*, 759–764.

(26) Shimada, N.; Kawamoto, H.; Saka, S. *J Anal. Appl. Pyrolysis* **2008**, *81*, 80–87.

(27) Collard, F.; Blin, J.; Bensakhria, A.; Valette, J. *J. Anal. Appl. Pyrolysis* **2012**, *95*, 213–226.

(28) Liaw, S. B.; Wu, H. *Ind. Eng. Chem. Res.* **2013**, *52*, 4280–4289.

(29) Liao, C.; Wu, C.; Yan, Y. *Fuel Process Technol.* **2007**, *88*, 149–156.

(30) Wu, H.; Yip, K.; Kong, Z.; Li, C.; Liu, D.; Yu, Y.; Gao, X. *Ind. Eng. Chem. Res.* **2011**, *50*, 12143–12151.

(31) Montgomery, D. C. *Design and analysis of experiments*; John Wiley & Sons: Hoboken, NJ, 2005.

(32) Grömping, U. *Tutorial for designing experiments using the R package RcmdrPlugin.DoE*; Report 4/2011; Reports in Mathematics, Physics and Chemistry; Beuth University of Applied Sciences: Berlin, Germany, 2011.

(33) He, F.; Yi, W.; Bai, X. *Energy Conversion Manage.* **2006**, *47*, 2461–2469.

(34) Van de Velden, M.; Baeyens, J.; Brems, A.; Janssens, B.; Dewil, R. *Renewable Energy* **2010**, *35*, 232–242.

(35) Yang, H.; Kudo, S.; Kuo, H.; Norinaga, K.; Mori, A.; Masek, O.; Hayashi, J. *Energy Fuels* **2013**, in press; DOI 10.1021/ef400199z.

(36) White, J. E.; Catallo, W. J.; Legendre, B. L. *J. Anal. Appl. Pyrolysis* **2011**, *91*, 1–33.

(37) Oyedun, A. O.; Gebreegziabher, T.; Hui, C. W. *Fuel Process Technol.* **2013**, *106*, 595–604.

(38) Khawam, A.; Flanagan, D. R. *J. Phys. Chem. B* **2006**, *110*, 17315–17328.

(39) Park, Y.; Kim, J.; Kim, S.; Park, Y. *Bioresour. Technol.* **2009**, *100*, 400–405.

(40) Biagini, E.; Fantei, A.; Tognotti, L. *Thermochimica Acta* **2008**, *472*, 55–63.

(41) Hu, S.; Jess, A.; Xu, M. *Fuel* **2007**, *86*, 2778–2788.

(42) Santos, K. G.; Lobato, F. S.; Lira, T. S.; Murata, V. V.; Barrozo, M. A. S. *Chem. Eng. Res. Design* **2012**, *90*, 1989–1996.

(43) Orfão, J. J. M.; Antunes, F. J. A.; Figueiredo, J. L. *Fuel* **1999**, *78*, 349–358.

(44) Venkataraman, P. *Applied Optimization with MATLAB Programming*; John Wiley & Sons: Hoboken (NJ), 2009.

(45) Johnson, M. L. Nonlinear Least-Squares Fitting Methods. In *Methods in Cell Biology*; Academic Press: New York; Vol. 84, pp 781–805.

Table 1. Proximate, elemental, and XRF analyses of both raw and washed TPOMW samples.

	Raw sample	*Washed sample*
Proximate (wt % db[1])		
Ash	2.73 ± 0.07	1.44 ± 0.11
Volatile Matter	76.50 ± 0.48	77.81 ± 0.46
Fixed Carbon	20.77 ± 1.36	20.75 ± 1.24
Ultimate (wt % daf[2])		
C	42.0 ± 1.05	41.6 ± 0.96
H	5.99 ± 0.06	6.01 ± 0.84
N	3.18 ± 0.12	3.21 ± 0.14
S	< 0.1	< 0.1
Inorganic matter (wt % of ash)		
CaO	42.1	34.1
K_2O	26.4	2.34
SiO_2	10.0	49.94
Fe_2O_3	6.90	3.34
Al_2O_3	3.91	1.04
P_2O_5	3.90	1.72
MgO	1.69	0.828
TiO_2	0.476	0.112
PbO	0.256	1.30
SnO_2	0.231	1.18
CuO	0.221	1.09
MnO	0.196	1.01
ZnO	0.137	0.689
SO_3	2.95	0.796
Cl	0.251	< 0.01

[1] Dry basis

[2] Dry and ash-free basis

Table 2. The 2_{IV}^{4-1} design followed in the present study.

Level	Factors				
	A	**B**	**C**	**D**	
	Sample mass (mg)	Heating rate (K min^{-1})	Crucible	Sample type	
Low (–1)	10	5	Without lid	Untreated	
High (+1)	40	25	With lid	Washed	
Run	Factors				Treatment
	A	**B**	**C**	**D**	
1	–1	–1	–1	–1	*(1)*
2	–1	+1	–1	+1	*bd*
3	–1	–1	+1	+1	*cd*
4	+1	–1	–1	+1	*ad*
5	+1	+1	–1	–1	*ab*
6	–1	+1	+1	–1	*bc*
7	+1	+1	+1	+1	*abcd*
8	+1	–1	+1	–1	*ac*
9	–1	–1	–1	–1	*(1)*
10	+1	+1	–1	–1	*ab*
11	–1	–1	+1	+1	*cd*
12	–1	+1	+1	–1	*bc*
13	–1	+1	–1	+1	*bd*
14	+1	–1	–1	+1	*ad*
15	+1	+1	+1	+1	*abcd*
16	+1	–1	+1	–1	*ac*

Table 3. Experimental results obtained for the fractional factorial design.

Run	Treatment	y_{char}	Q_{exp} (kJ kg^{-1})[3]	T_{max} (ºC)
1	(1)	0.3486	2440	320.9
2	*bd*	0.3632	1238	336.5
3	*cd*	0.3768	–12.5	337.0
4	*ad*	0.3760	120.6	329.4
5	*ab*	0.3149	83.0	331.2
6	*bc*	0.3103	–75.7	363.5
7	*abcd*	0.4138	–14.1	358.4
8	*ac*	0.3921	–0.8	332.4
9	*(1)*	0.3617	2678	324.0
10	*ab*	0.3517	83.6	337.6
11	*cd*	0.3411	–79.7	339.0
12	*bc*	0.3514	–139.5	360.5
13	*bd*	0.3350	1538	339.6
14	*ad*	0.3526	50.2	328.5
15	*abcd*	0.4257	–10.1	357.9
16	*ac*	0.3878	–21.1	332.4

[3] Heat per unit of dry initial sample mass (m_{bio}).

Table 4. Regression coefficients and ANOVA table (response variable: Q_{exp}).

Regression coefficients

Term	Effect	Coefficient	Std. Error	*t* value	*p*-value
(Intercept)		492.4	24.99	19.7	0.000
A	–911.9	–456.0	24.99	–18.25	0.000
B	–309.0	–154.5	24.99	–6.18	0.000
C	–1073.1	–536.6	24.99	–21.47	0.000
D	–277.2	–138.6	24.99	–5.55	0.001
AB (+ CD)	307.3	153.7	24.99	6.15	0.000
AC (+ BD)	977.3	488.6	24.99	19.55	0.000
AD (+ BC)	277.6	138.8	24.99	5.56	0.001

Residual standard error: 99.96 on 8 degrees of freedom; R^2: 0.9939; Adjusted R^2: 0.9887

F-statistic: 187.7 on 7 and 8 DF; *p-value* = 3.109e–8

ANOVA table

Source	DF	Sum of squares	Mean squares	*F* value	*p*-value
Main effects	4	8622241	2155560	215.73	0.000
A	1		3326520	332.92	0.000
B	1		381893	38.22	0.000
C	1		4606496	461.03	0.000
D	1		307332	30.76	0.001
2-way interactions	3	4506519	1502173	150.34	0.000
AB (+ CD)	1		377825	37.81	0.000
AC (+ BD)	1		3820363	382.35	0.000
AD (+ BC)	1		308330	30.83	0.001
Pure error	8	79935	9992		
Total	15	13208695			

Table 5. Regression coefficients and ANOVA table (response variable: y_{char}).

Regression coefficients

Term	Effect	Coefficient	Std. Error	*t* value	*p*-value
(Intercept)		0.3627	0.0048	74.96	0.000
A	0.0283	0.0142	0.0048	2.93	0.019
B	–0.0088	-0.0044	0.0048	–0.91	0.388
C	0.0244	0.0122	0.0048	2.52	0.036
D	0.0207	0.0104	0.0048	2.14	0.065
AB (+ CD)	0.0082	0.0041	0.0048	0.85	0.419
AC (+ BD)	0.0316	0.0158	0.0048	3.27	0.011
AD (+ BC)	0.0097	0.0048	0.0048	1.00	0.346

Residual standard error: 0.0194 on 8 degrees of freedom; R^2: 0.8037; Adjusted R^2: 0.6319

F-statistic: 4.678 on 7 and 8 DF; *p-value* = 0.0228

ANOVA table

Source	DF	Sum of squares	Mean squares	*F* value	*p*-value
Main effects	4	0.0076	0.0019	5.09	0.025
A	1	0.0032	0.0032	8.56	0.019
B	1	0.0003	0.0003	0.83	0.388
C	1	0.0024	0.0024	6.37	0.036
D	1	0.0017	0.0017	4.58	0.065
2-way interactions	3	0.0046	0.0016	4.14	0.048
AB (+ CD)	1	0.0003	0.0003	0.72	0.419
AC (+ BD)	1	0.0040	0.0040	10.69	0.011
AD (+ BC)	1	0.0004	0.0004	1.00	0.346
Pure error	8	0.0030	0.0004		
Total	15	0.0153			

Table 6. Regression coefficients and ANOVA table (response variable: T_{max}).

Regression coefficients

Term	Effect	Coefficient	Std. Error	*t* value	*p*-value
(Intercept)		339.3	0.5385	930.06	0.000
A	–1.650	–0.825	0.5385	–1.53	0.164
B	17.700	8.850	0.5385	16.43	0.000
C	16.675	8.337	0.5385	15.48	0.000
D	2.975	1.487	0.5385	2.76	0.025
AB (+ CD)	–2.100	–1.050	0.5385	–1.95	0.087
AC (+ BD)	–3.075	–1.538	0.5385	–2.86	0.021
AD (+ BC)	7.175	3.587	0.5385	6.66	0.000

Residual standard error: 2.154 on 8 degrees of freedom; R^2: 0.9863; Adjusted R^2: 0.9743

F-statistic: 82.3 on 7 and 8 DF; *p-value* = 8.032e–7

ANOVA table

Source	DF	Sum of squares	Mean squares	*F* value	*p*-value
Main effects	4	2411.68	602.92	129.94	0.000
A	1	10.89	10.89	2.35	0.164
B	1	1253.16	1253.16	270.08	0.000
C	1	1112.22	1112.22	239.70	0.000
D	1	35.40	35.40	7.63	0.025
2-way interactions	3	261.38	87.13	18.78	0.001
AB (+ CD)	1	17.64	17.64	3.80	0.087
AC (+ BD)	1	37.82	37.82	8.15	0.021
AD (+ BC)	1	205.92	205.92	44.38	0.000
Pure error	8	37.12	4.64		
Total	15	2710.18			

Table 7. List of the model parameters for the kinetics of TPOMW pyrolysis, deduced from some experiments conducted at 5 K min^{-1}. Values in brackets correspond to the starting values provided to the optimization procedure.

Parameter	Run #1	Run #4	Run #11	Run #16
c_1	0.1189 (0.1185)	0.1156 (0.2071)	0.1232 (0.1177)	0.1100 (0.1071)
c_2	0.2115 (0.1995)	0.2100 (0.1350)	0.2193 (0.2094)	0.1990 (0.1886)
c_3	0.3211 (0.3334)	0.3120 (0.2819)	0.3355 (0.3178)	0.3270 (0.3016)
$log\ A_1$ (A_1 in s^{-1})	8.009 (8.848)	7.994 (7.486)	8.006 (7.962)	7.928 (7.744)
$log\ A_2$ (A_2 in s^{-1})	12.44 (12.66)	12.43 (12.54)	12.46 (12.48)	12.43 (12.59)
$log\ A_3$ (A_3 in s^{-1})	0.2672 (2.458)	0.7263 (3.404)	0.2122 (1.956)	0.3729 (2.612)
$log\ A_4$ (A_4 in s^{-1})	n.d.	2.243 (1)	2.228 (1)	2.182 (1)
$E1$ (kJ mol^{-1})	117.0 (118.2)	118.9 (107.3)	120.3 (111.9)	117.3 (119.3)
$E2$ (kJ mol^{-1})	173.8 (170.3)	176.6 (285.2)	179.5 (302.6)	175.8 (177.3)
$E3$ (kJ mol^{-1})	45.17 (62.22)	49.74 (75.22)	44.8 (65.4)	48.06 (59.21)
$E4$ (kJ mol^{-1})	n.d.	97.90 (1)	100.6 (1)	100.7 (1)
n_1	1.51 (0.92)	0.95 (1.10)	0.99 (1.08)	1.34 (1.11)
n_2	1.64 (1.09)	1.24 (1.27)	1.18 (1.25)	1.52 (1.31)
n_3	1.77 (2.28)	2.18 (2.57)	1.99 (2.79)	1.95 (2.05)
n_4	n.d.	1.16 (1)	1.15 (1)	1.18 (1)
γ	n.d.	0.0301 (1)	0.0479 (1)	0.1020 (1)
FPE	$2.34\ 10^{-6}$	$2.54\ 10^{-6}$	$3.69\ 10^{-6}$	$3.51\ 10^{-6}$
R^2_{adj}	0.9940	0.9908	0.9902	0.9913
CPU time[4] *(s)*	345	389	1385	568

[4] Intel© Core i5 2430M at 2500 MHz; 6 GB RAM.

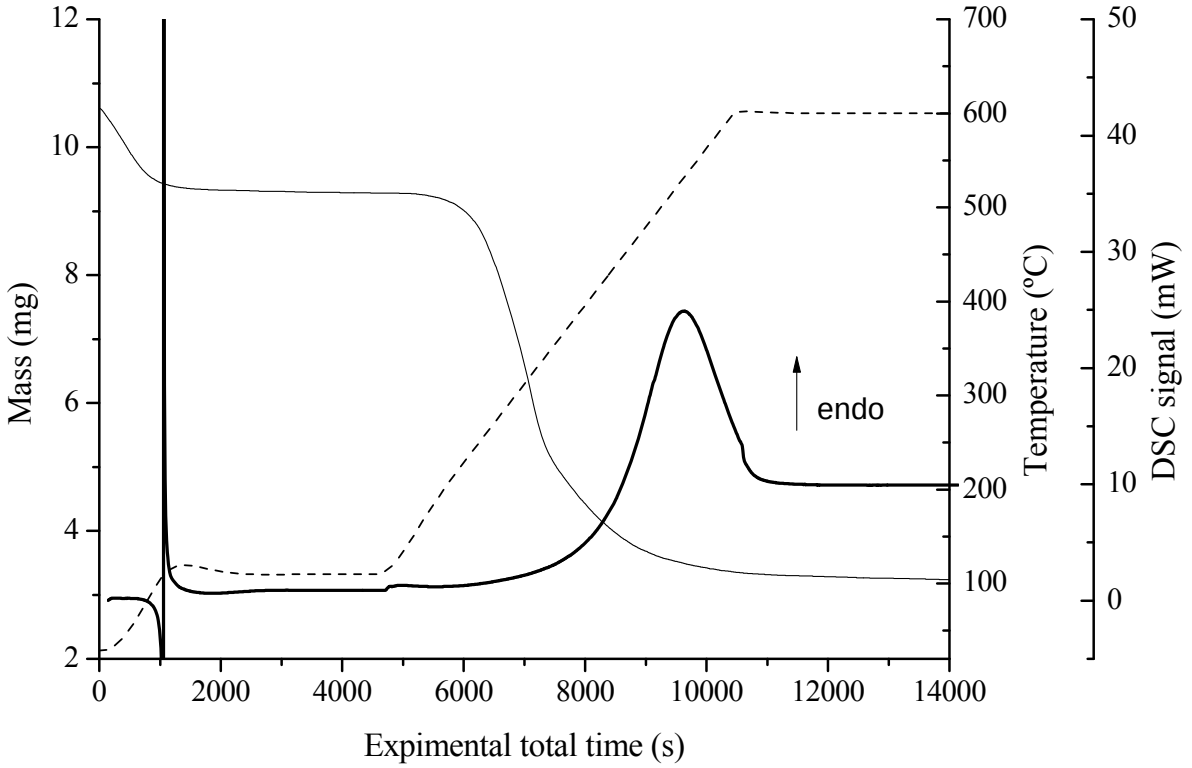

"**Figure 1.** An example of TG and DSC curve (run #1): solid line (mass); dashed line (temperature); and bold solid line (DSC signal)."

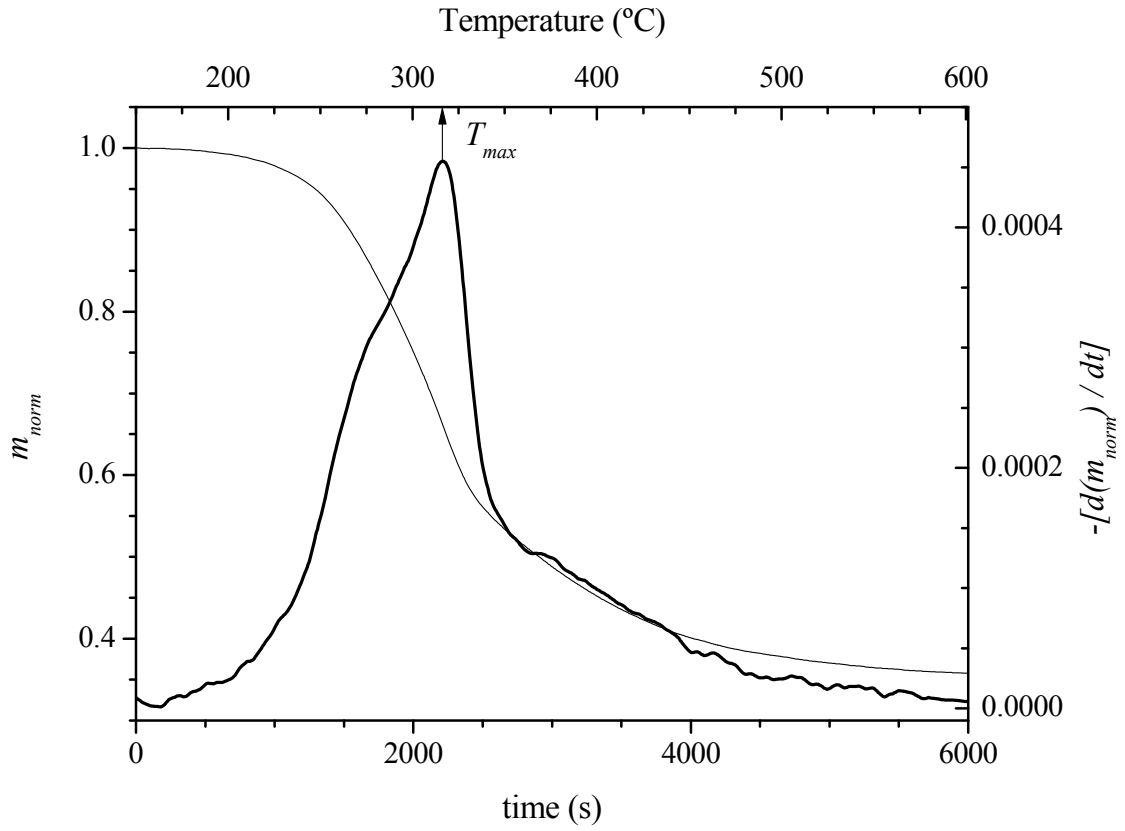

"**Figure 2.** An example of normalized TG and DTG curve (run #1): solid line (normalized mass); bold solid line (–DTG)."

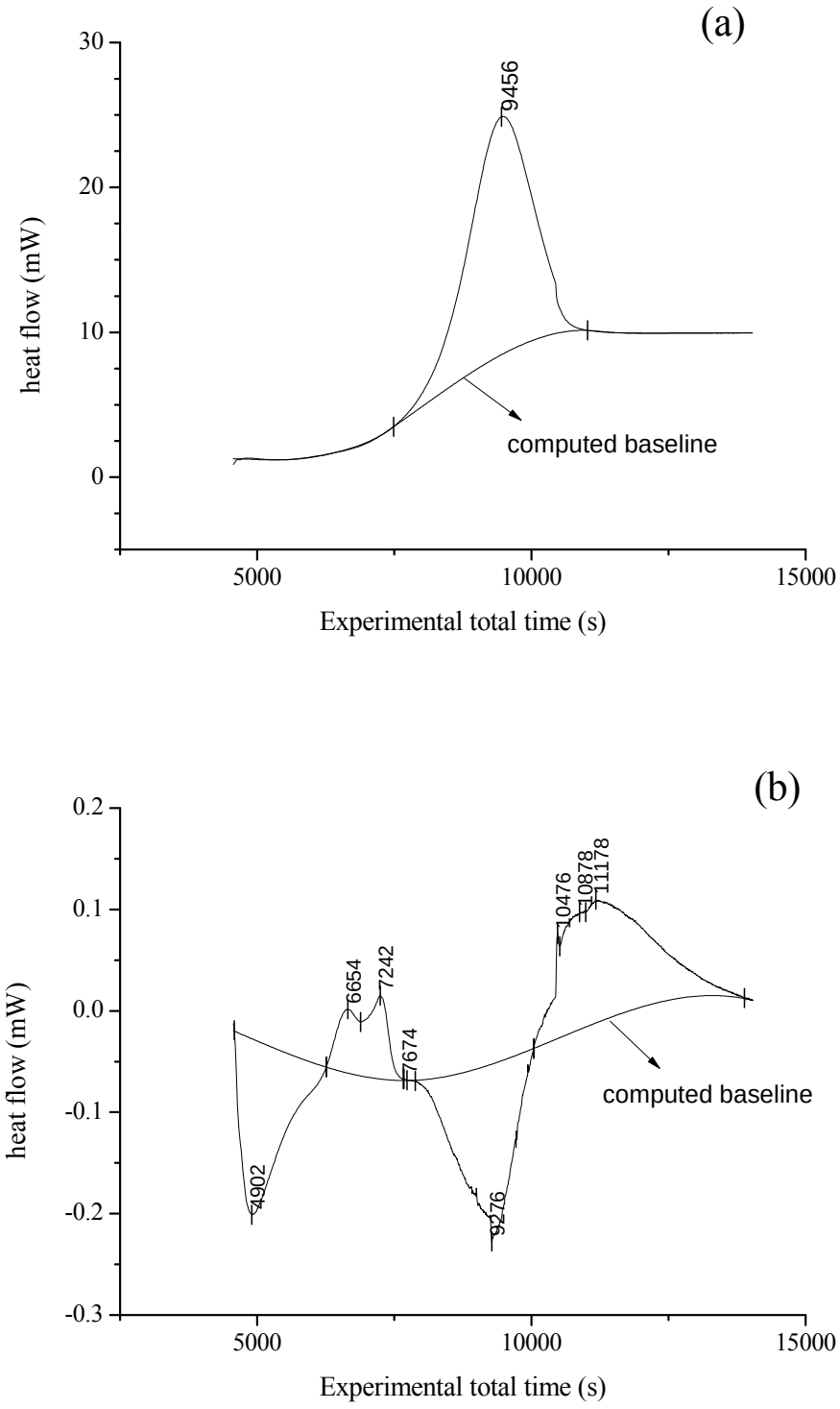

"**Figure 3.** Two examples of DSC signal processing: (a), run #1; (b); run #8."

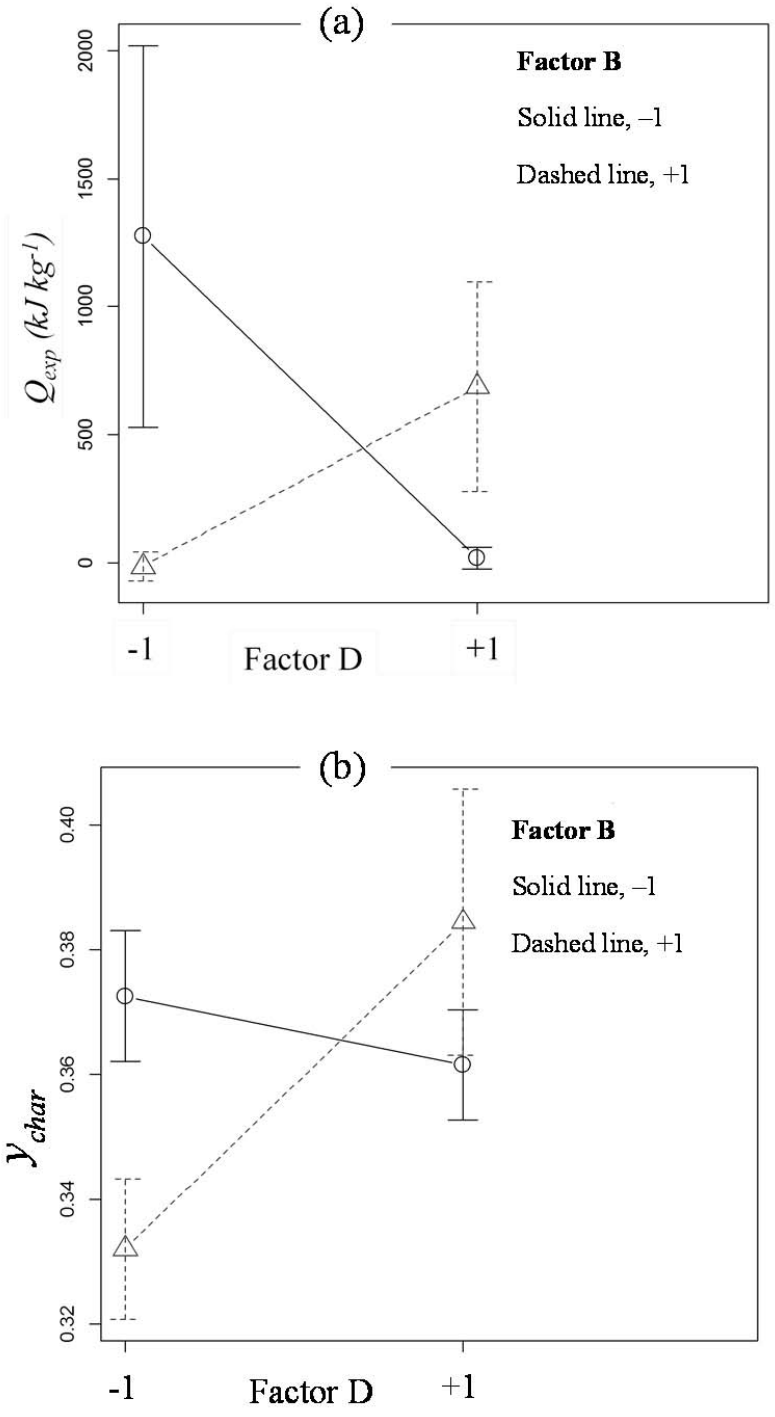

"**Figure 4.** Two-way interaction plot of the impact of factors B and D on (a), the average Q_{exp} response and (b), the average y_{char} response."

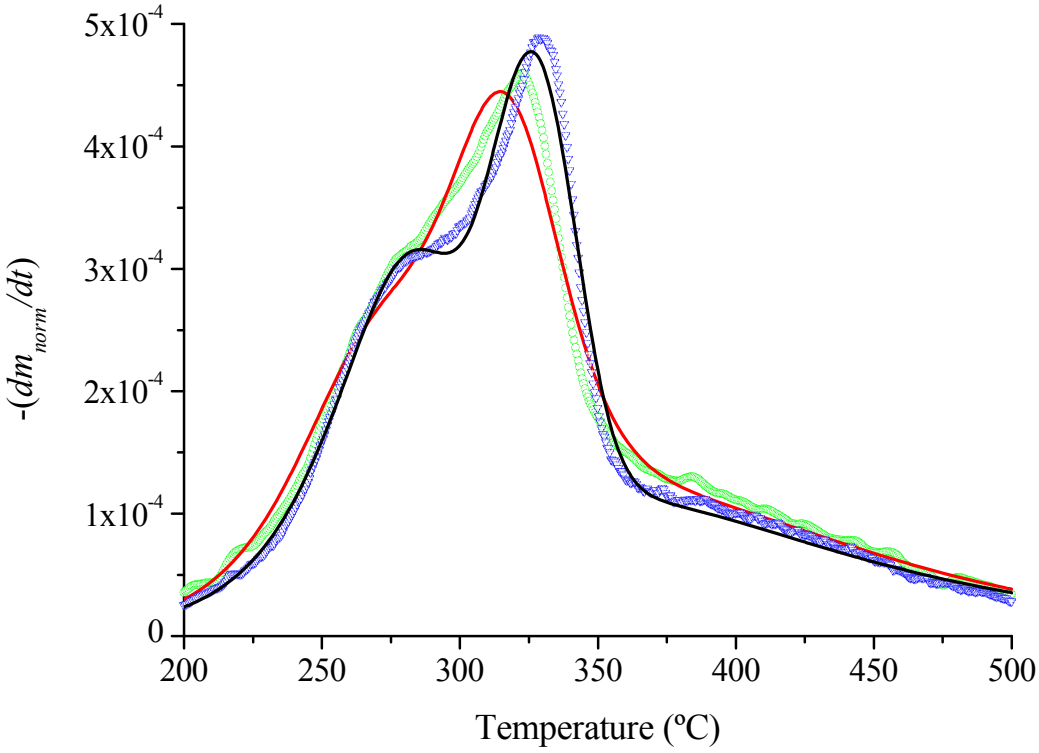

"**Figure 5.** Comparison of the experimental DTG curves and the simulated ones for run #1 (green circle, experimental data; red line, calculated data) and run #4 (blue triangle, experimental data; black line, calculated data)."

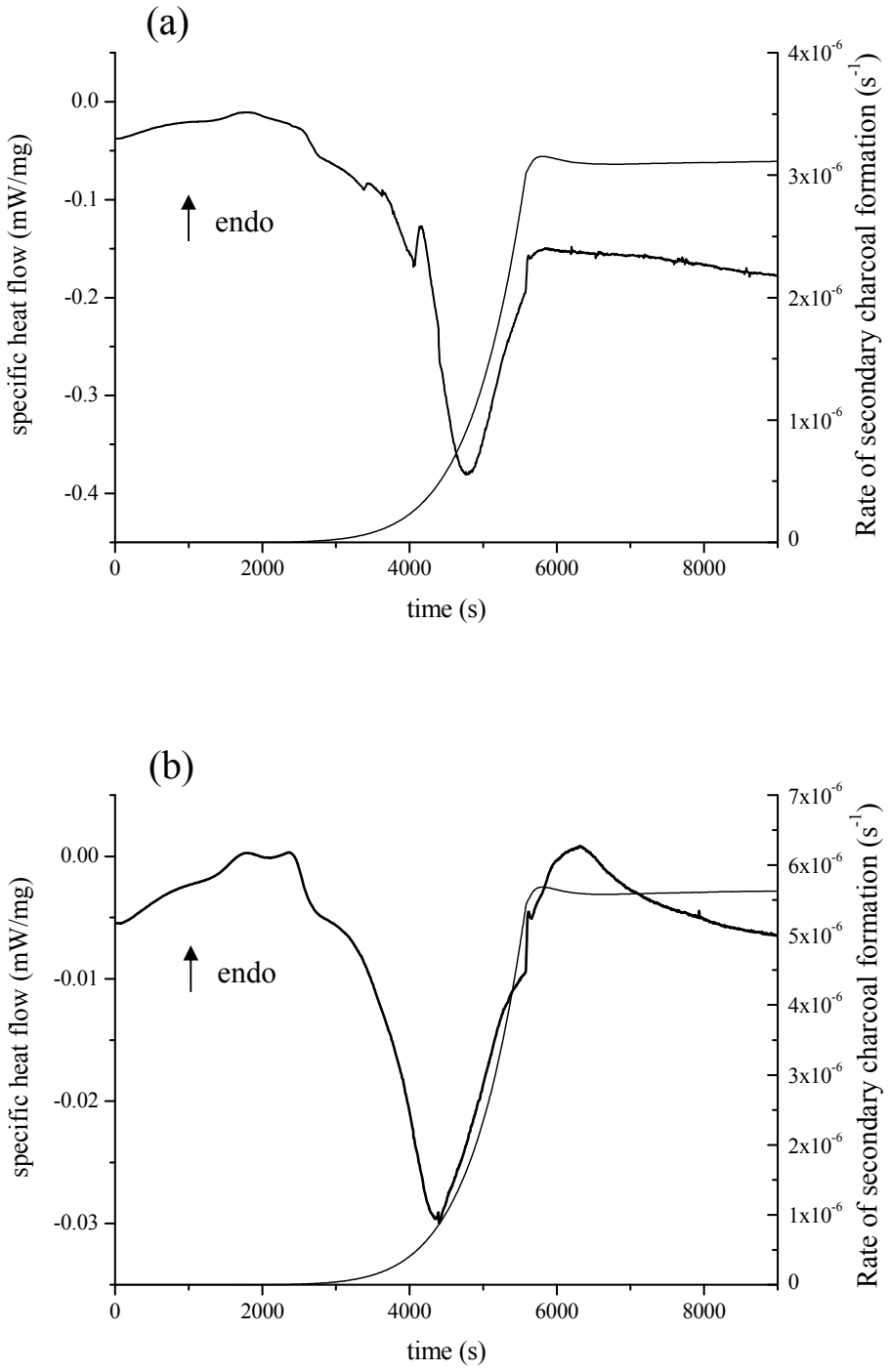

"**Figure 6.** Evolution of the specific heat flow (bold solid line) and the rate of secondary charcoal formation (solid line): (a), run #11; (b); run #16."